Optimal energy management under spatio-temporal constraints: an application to solar-powered vehicles

Control Engineering Practice 173 (2026) 106964

Contents lists available at ScienceDirect

Control Engineering Practice

journal homepage: www.elsevier.com/locate/conengprac

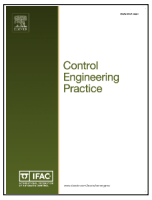

Optimal energy management under spatio-temporal constraints: An application to solar-powered vehicles

Lorenzo Montalto [a,*], Nikolce Murgovski [a], Timothy Jarebrant [b]

[a] Department of Electrical Engineering, Chalmers University of Technology, Sweden
[b] Chalmers Solar Team, Chalmers University of Technology, Sweden

ARTICLE INFO

Keywords:
Optimal control
Non-linear control systems
Automotive control
Transportation systems

ABSTRACT

This paper addresses a nonlinear optimal control problem for mission planning of long-range solar-powered electric vehicles to optimize trip time and energy management while subject to spatio-temporal constraints. The problem is formulated using first-principles modeling and solved through direct multiple shooting. The output is a driving profile that minimizes trip time while guaranteeing journey completion, constraint compliance and differentiability. The method is applied to a vehicle competing in the Bridgestone World Solar Challenge, a 3 022 km race across Australia, where the spatio-temporal constraints arise from the competition's rules. Simulation results are compared with telemetric data collected during the competition.

1. Introduction

A great challenge of our time is climate change, and a particularly critical sector is transport, having the second highest CO2 emissions by sector (Ritchie et al., 2020). Sobczuk and Borucka (2024) provide a review of recent research on making the transport sector more sustainable.

Electric vehicles (EVs) are often mentioned as a greener alternative to internal combustion engine vehicles (ICEVs). While that is true under certain conditions (Kish, 2023), some issues discourage their adoption. One is range anxiety, i.e. the fear of depleting the battery before reaching a charging station, since EVs have a shorter range compared to ICEVs (Pevec et al., 2019). One way to address this, without resorting to a larger battery, is by improving the vehicle's energy efficiency by optimizing its driving profile, such that it guarantees reaching the destination while minimizing energy consumption. This is known as eco-driving (Huang et al., 2018).

The eco-driving problem can be formulated as an optimal control problem (OCP), solvable through many known techniques. One is Dynamic Programming (DP), as in Li et al. (2022). However, DP suffers from the curse of dimensionality, making it computationally infeasible even for reasonably-sized problems. Deshpande et al. (2022) solves the OCP through DP in a computationally tractable way, using a Model Predictive Control (MPC) framework in which DP is applied over a shorter prediction horizon rather than the entire mission. An alternative tractable way to solve MPCs is direct multiple shooting (Kiehl, 1994), a numerical method to solve OCPs' boundary value problems, used by, e.g., Li et al. (2024), to solve the eco-driving problem.

When solving the eco-driving problem with multiple shooting methods, location-triggered stops (LTS, e.g., recharging at a station whose location is known) and time-triggered stops (TTS, e.g., the driver stopping to rest after several hours of driving) might give rise to spatio-temporal constraints which pose modeling challenges. The dynamics of the system are different when the vehicle is driving and when it is standing still (and possibly recharging). To address LTS in a tractable manner, Hamednia et al. (2023) propose changing the domain from space to time (i.e., changing the independent variable that all other signals are functions of) when the vehicle switches from driving to charging mode. However, this is tricky to achieve if the location where the switch occurs is not known, which is the case for TTS. Another way is having integer variables that indicate whether the vehicle is driving or not, but that would make the problem mixed-integer, which is computationally more demanding than a continuous one. Finally, planning for a solar-powered EV requires taking into account the weather forecast, which also requires keeping track of the current day and hour.

A common technique in multiple-shooting methods is first principles modeling, in which mathematical models are created using fundamental physical laws and principles. In this study, first principles modeling is used to formulate a nonlinear minimum-time OCP for a long-mission planning of solar-powered EV, subject to optimal energy management and spatio-temporal constraints (LTS and TTS). The challenge of

* Corresponding author.
E-mail address: lorenzo.montalto@chalmers.se (L. Montalto).

https://doi.org/10.1016/j.conengprac.2026.106964
Received 2 November 2025; Received in revised form 12 February 2026; Accepted 23 March 2026

modeling both kinds of stops without shifting between space and time domains or using integer variables, while still preserving differentiability, is a core contribution of this work.

The proposed method was validated in a case study by optimizing the driving profile of an EV competing in the Bridgestone World Solar Challenge (BWSC), a 3 022 km race for solar-powered vehicles across the Australian Outback. The OCP was solved numerically through direct multiple shooting. Although the competition is a race, the vehicle being entirely solar-powered makes simply reaching the destination already challenging, making energy efficiency essential, even more so since the competition in 2025 took place during winter. This resulted in a reduction of about 20% in available sun hours and a higher chance of inclement weather. Both challenges are of great interest, as one of the main concerns regarding solar power is its fluctuation depending on the weather (Billinton & Bagen, 2006). The results of the competition are compared with those obtained through simulation.

The rest of the article is structured as follows. Section 2 formulates the optimization problem and the model for a solar-powered EV. Section 3 describes how the OCP is reformulated in space domain and how differentiability issues in the original formulation are addressed. Section 4 provides a mathematical model for charging using solar power. Section 5 shows the results of the method applied in the case study. Finally, Section 6 sums up the main findings of the article and provides some conclusions and ideas for future developments.

2. Problem formulation

In this section, the minimum-time OCP, subject to spatio-temporal constraints and energy efficiency requirements, is formulated for a solar-powered EV. The problem is formulated in time domain, with the following states, control inputs and parameters

$$\mathbf{x}(t) = \begin{bmatrix} \tau(t) & s(t) & E_\mathrm{k}(t) & \mathrm{SoC}(t) \end{bmatrix}^\intercal \tag{1a}$$

$$u(t) = a(t) \tag{1b}$$

$$\mathbf{p}(t,s) = \begin{bmatrix} \theta(s) & P_\mathrm{sol}(t,s) \end{bmatrix}^\intercal \tag{1c}$$

where t is the absolute time, τ is the driving time, s is the position, E_k is the kinetic energy for a unitary mass (i.e., $\sqrt{2E_k}$ is the vehicle speed), SoC is the state of charge, a is the traction acceleration (negative when braking), θ is the terrain's slope and P_sol is the solar power. The states dynamics can then be defined as

$$\frac{\mathrm{d}\tau(t)}{\mathrm{d}t} = \begin{cases} 1, & \text{if } t \notin \mathbb{T}_\mathrm{stop} \text{ and } s(t) \notin \mathbb{S}_\mathrm{stop} \\ 0, & \text{otherwise} \end{cases} \tag{2a}$$

$$\frac{\mathrm{d}s(t)}{\mathrm{d}t} = \sqrt{2E_\mathrm{k}(s)} \tag{2b}$$

$$\frac{\mathrm{d}E_\mathrm{k}(t)}{\mathrm{d}t} = \sqrt{2E_\mathrm{k}(s)} \cdot \left(a(t) - \frac{F_\mathrm{drag}(t)}{m} - g\ \sin(\theta(t)) + \right. \\ \left. - C_\mathrm{r}\ g\ \cos(\theta(t)) \right) \tag{2c}$$

$$\frac{\mathrm{dSoC}(t)}{\mathrm{d}t} = -\frac{P_\mathrm{b}(t)}{C_\mathrm{b} V_\mathrm{oc}(\mathrm{SoC})} \tag{2d}$$

where $\mathbb{T}_\mathrm{stop}$ and $\mathbb{S}_\mathrm{stop}$ are, respectively, the sets of the times and locations for the TTS and the LTS (known in advance), F_drag is the aerodynamic drag force along the longitudinal axis, m is the vehicle's mass, g is the gravitational acceleration, C_r is the rolling resistance coefficient, P_b is the battery's internal chemical power (negative when charging and positive otherwise), V_oc is the battery's open circuit voltage, and C_b is the battery capacity. The sets $\mathbb{T}_\mathrm{stop}$ and $\mathbb{S}_\mathrm{stop}$ are defined as

$$\mathbb{T}_\mathrm{stop} = \cup_i\ [t_{i,0}, t_{i,\mathrm{f}}] \tag{3a}$$

$$\mathbb{S}_\mathrm{stop} = \cup_i\ \{s_i^\mathrm{stop}\} \tag{3b}$$

where $t_{i,0}$ and $t_{i,\mathrm{f}}$ are the time instants when the i^{th} TTS starts and ends, respectively, and s_i^stop is the location of the i^{th} LTS. The constraint (2a) states that the driving time does not increase during LTS and TTS.

The aerodynamic drag force along the longitudinal axis is defined as

$$F_\mathrm{drag}(E_\mathrm{k}) = \frac{1}{2} \rho_\mathrm{air} c_\mathrm{D} A_\mathrm{f} v_\mathrm{rel}(E_\mathrm{k}) |v_\mathrm{rel}(E_\mathrm{k})| \tag{4}$$

where ρ_air is the air density, c_D is the drag coefficient, A_f is the vehicle's frontal area and v_rel is the relative velocity of the vehicle with respect to the apparent wind along its path, computed as

$$v_\mathrm{rel}(t) = \sqrt{2E_\mathrm{k}} - \alpha_\mathrm{w} w_\mathrm{eff}(t) \tag{5}$$

where α_w is an altitude-dependent coefficient and w_eff is the effective along-track wind, obtained through satellite data. If $v_\mathrm{rel}(t) > 0$, the vehicle is driving headwind.

The following power balance equation holds for the system

$$P_\mathrm{sol}(t,s) + P_b(\mathbf{x},u) = P_\mathrm{prop}(a, E_\mathrm{k}) + P_\mathrm{joule}(P_\mathrm{b}, \mathrm{SoC}) \tag{6}$$

where P_prop is the propulsion power and P_joule is the power lost due to joule losses.

The full minimum-time OCP subject to given spatio-temporal constraints can then be formulated as

$$\min_{\mathbf{x},\mathbf{u}}\ \tau(t_\mathrm{f}) \tag{7a}$$

$$\text{s.t.: } \mathbf{x}(0) = \mathbf{x}_0,\ (2), (6) \tag{7b}$$

$$\mathbf{x}_\mathrm{min} \le \mathbf{x}(t) \le \mathbf{x}_\mathrm{max},\ t \in [0, t_\mathrm{f}] \tag{7c}$$

$$u_\mathrm{min} \le u(t) \le u_\mathrm{max},\ t \in [0, t_\mathrm{f}] \tag{7d}$$

where $\mathbf{x}_0$ is some known initial condition, t_f is the final time, $\mathbf{x}_\mathrm{min}$ and $\mathbf{x}_\mathrm{max}$ are, respectively, the vectors of lower and upper bounds for the states and u_min and u_max are, respectively, the lower and upper bounds for the acceleration.

Several aspects of problem (7) make it difficult to handle. Since it is a minimum-time OCP, the total driving time $\tau(t_\mathrm{f})$, and therefore the total absolute time t_f, are not known in advance. Furthermore, to model (2a) we need to distinguish between when the vehicle is driving and when it is not. This is also true for (6), since the battery power and the joule losses are different when charging and discharging. If the electric motor's efficiency is different when the vehicle accelerates ($a > 0$) and when it brakes ($a < 0$), (2c) would also need to be piece-wise defined to distinguish the two cases. Finally, (4) includes an absolute value function, which creates differentiability problems.

In the next section, a method is formulated to solve this problem without needing integer variables or to switch between time and space domain, while still preserving differentiability. The presented method is general and can be applied to minimize the trip time for any solar-powered EV under given spatio-temporal constraints.

3. Reformulation in space domain

Since both TTS and LTS are imposed, choosing to model the problem in either time or space domain facilitates one at the expense of the other. We chose to model the problem in space domain, so that the location s in (1a) can be removed from the state vector.

To avoid defining (2c) in a piece-wise manner, we split the acceleration a into two signals, one for (positive) acceleration a^+ and one for braking a^-, such that the total acceleration a is the sum of the two. This works as long as the two signals cannot both be non-zero at the same time, but that would never happen, as accelerating and braking at the same time would be a waste of energy, and the optimal solution has no incentive to support that.

Finally, to remove the absolute value function from (4), we define a dummy control input F_drag and the two following additional constraints

$$F_\mathrm{drag}(s) \ge \frac{1}{2} \rho_\mathrm{air} c_\mathrm{D} A_\mathrm{f} v_\mathrm{rel}^2(E_\mathrm{k}) \tag{8a}$$

$$F_\mathrm{drag}(s) \ge -\frac{1}{2} \rho_\mathrm{air} c_\mathrm{D} A_\mathrm{f} v_\mathrm{rel}^2(E_\mathrm{k}). \tag{8b}$$

This appears to be a relaxation of (4), but it still leads to an exact solution, because depending on the sign of v_{rel}, one of the two inequalities should hold with equality at the optimum. We would essentially have

$$F^*_{\text{drag}}(s) = \begin{cases} \frac{1}{2}\rho_{\text{air}} c_{\text{D}} A_{\text{f}} v^2_{\text{rel}}(E^*_{\text{k}}), & \text{if } v_{\text{rel}} \geq 0 \\ -\frac{1}{2}\rho_{\text{air}} c_{\text{D}} A_{\text{f}} v^2_{\text{rel}}(E^*_{\text{k}}), & \text{if } v_{\text{rel}} < 0. \end{cases} \tag{9}$$

Otherwise, the aerodynamic drag would be higher than strictly necessary, which, similarly as discussed above, would be a waste of energy.

The states, the control inputs and the parameters in space domain are then defined as

$$\mathbf{x}(s) = \begin{bmatrix} \tau(s) & E_{\text{k}}(s) & \text{SoC}(s) \end{bmatrix}^\intercal \tag{10a}$$

$$\mathbf{u}(s) = \begin{bmatrix} a^+(s) & a^-(s) & F_{\text{drag}}(s) \end{bmatrix}^\intercal \tag{10b}$$

$$\mathbf{p}(s,t) = \begin{bmatrix} \theta(s) & P_{\text{sol}}(s,t) \end{bmatrix}^\intercal. \tag{10c}$$

The states and the control inputs are bounded as

$$[0,\ \frac{v^2_{\text{min}}(s)}{2},\ \text{SoC}_{\text{min}}]^\intercal \leq \mathbf{x}(s) \leq [\tau_{\text{max}},\ \frac{v^2_{\text{max}}(s)}{2},\ \text{SoC}_{\text{max}}]^\intercal$$

$$[0,\ a_{\text{min}}(E_{\text{k}}), -F^{\text{max}}_{\text{drag}}]^\intercal \leq \mathbf{u}(s) \leq [a_{\text{max}}(E_{\text{k}}),\ 0,\ F^{\text{max}}_{\text{drag}}]^\intercal$$

where a_{min} and a_{max} are the lower and upper bounds for the acceleration, $\text{SoC}_{\text{min}} \geq 0$ and $\text{SoC}_{\text{max}} \leq 1$ are the lower and upper bounds for the SoC, τ_{max} is an upper bound for the driving time, v_{min} and v_{max} are, respectively, the lower and upper bound for the speed of the vehicle, and $F^{\text{max}}_{\text{drag}}$ is an upper bound for the dummy control input, defined as

$$F^{\text{max}}_{\text{drag}} = \frac{\rho_{\text{air}} c_{\text{D}} A_{\text{f}} v_{\text{max}}}{2}. \tag{11}$$

The bounds on the SoC are sometimes used to prevent the battery from being charged too much (as then charging becomes slow) or to make sure that the SoC does not drop too much (for robustness). This is the case when the upper bound is less than 1 and the lower bound is greater than 0. In such cases, the bounds can be relaxed to aid convergence. To this aim, we define

$$\boldsymbol{\epsilon}_x(s) = [0,\ 0,\ \epsilon_{\text{SoC}}(s)]^\intercal \tag{12}$$

such that

$$\mathbf{x}_{\text{min}} \leq \mathbf{x}(s) + \boldsymbol{\epsilon}_x(s) \leq \mathbf{x}_{\text{max}},\ s \in [0, s_{\text{f}}] \tag{13}$$

where $\mathbf{x}_{\text{min}}$ and $\mathbf{x}_{\text{max}}$ are, respectively, the vectors of lower and upper bounds for the states, and s_{f} is the final location. Larger slack values indicate greater constraint "violation". Thus, they should be as close as possible to zero. We define the following cost function, which penalizes both driving time and constraint violation

$$J(s) = \tau(s_{\text{f}}) + \mu_\epsilon \int_0^{s_{\text{f}}} ||\boldsymbol{\epsilon}_x(s)|| \text{d}s \tag{14}$$

where μ_ϵ is a penalty for violating state constraints, and $||\cdot||$ indicates an appropriate vector norm. Since the second term is related to constraint violation, μ_ϵ is, in general, very high. That is because, even though the bounds on the states have been relaxed to aid convergence, they should still be treated as constraints, meaning that any violation should be heavily penalized.

The dynamics in space domain can be defined as

$$\frac{\text{d}\tau(s)}{\text{d}s} = \frac{1}{\sqrt{2E_{\text{k}}(s)}},\ \forall s \in \mathbb{S}_{\text{drv}} \tag{15a}$$

$$\frac{\text{d}E_{\text{k}}(s)}{\text{d}s} = a_+(s) + a_-(s) - \frac{F_{\text{drag}}(s)}{m} - g\ \sin(\theta(s)) - C_{\text{r}}\ g\ \cos(\theta(s)),\ \forall s \in \mathbb{S}_{\text{drv}} \tag{15b}$$

$$\frac{\text{dSoC}(s)}{\text{d}s} = -\frac{P_{\text{b}}(s)}{C_{\text{b}} V_{\text{oc}}(s)\sqrt{2E_{\text{k}}(s)}},\ \forall s \in \mathbb{S}_{\text{drv}} \tag{15c}$$

where $\mathbb{S}_{\text{drv}}$ is the locations where the vehicle is driving (i.e. not standing still), defined as

$$\mathbb{S}_{\text{drv}} = [0, s_{\text{f}}] \setminus \left(\mathbb{S}_{\text{stop}} \cup \{s : t(\tau(s)) \in \mathbb{T}_{\text{stop}}\}\right). \tag{16}$$

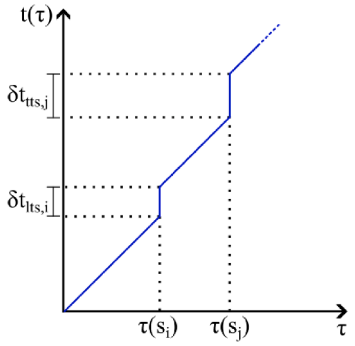

Fig. 1. Exemplified representation of the absolute time t as a function of the driving time τ.

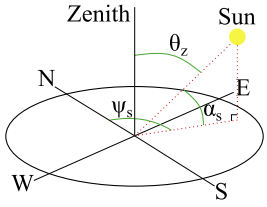

Fig. 2. Schematic of the key angles used to define the Sun's position in the sky.

The way the battery is charged during the stops is dealt with separately in Section 4.

The amount of available sunlight is not only a function of space but also of day and hour. Therefore, it is necessary to keep track of the absolute time t, which evolves as a function of τ according to Fig. 1, where $s_i \in \mathbb{S}_{\text{stop}}$ is the location of the i^{th} LTS, $s_j \in \{s : \tau(s) \in \mathbb{T}_{\text{stop}}\}$ is the location of the j^{th} TTS, and $\delta t_{\text{lts},i}$ and $\delta t_{\text{tts},j}$ are, respectively, the durations of the LTS and the TTS.

The following section addresses the computation of P_{sol}, which is then plugged in (6) to compute P_{b} and charge the battery according to (15c).

4. Solar power and energy

When dealing with solar energy calculations, one needs to keep track of several angles. Fig. 2 (a reproduction of a figure from Zhang et al. (2021)) should be used as a reference for the angles named in the following paragraphs.

According to (15c) and (6), the battery is recharged by the solar power P_{sol}, which is computed as the sum between the power obtained while driving and the one obtained during the TTS

$$P_{\text{sol}}(s) = P_{\text{drv}}(s) + P_{\text{tts}}(s). \tag{17}$$

This allows capturing the SoC variation during the TTS, even though the dynamics are in space domain and the vehicle is standing still. The vehicle can also be recharged during the LTS and that will be addressed later in this section.

The following subsections address the computation of P_{drv} and P_{tts}.

4.1. Solar irradiance

The powers P_{drv} and P_{tts} are obtained through solar irradiance. Their derivation requires first computing the total electrical power generated from solar irradiance, as

$$P_{\text{sun}}(s,t) = I_{\text{sun}}(s,t) \cdot A_{\text{p}} \cdot \eta_{\text{p}} \tag{18}$$

where A_{p} is the panel's surface area, η_{p} is the panel's efficiency, and I_{sun} is the total solar irradiance, computed as the sum of three contributions

$$I_{\text{sun}}(s,t) = I_{\text{dir}}(s,t) + I_{\text{dif}}(s,t) + I_{\text{alb}}(s,t) \tag{19}$$

where I_{dir}, I_{dif} and I_{alb} are, respectively, the solar irradiance from direct sunlight, from the Sun's rays being scattered by the atmosphere, and from the reflection of sunlight on the ground. The three types of irradiance will be addressed individually.

The first and greatest contribution to solar irradiance is from direct sunlight and is defined as

$$I_{\text{dir}}(s,t) = \max\big(0,\ I_{\text{n}}(s,t)\cos\gamma(s,t)\big) \tag{20}$$

where I_{n} is the direct normal irradiance, i.e. the insolation measured at a given location on Earth with a surface element (in this case, the panels) perpendicular to the Sun's rays (Kirk, 2014), and γ is the angle of incidence between the Sun's rays and the vehicle, whose cosine can be computed as

$$\begin{aligned}\cos\gamma(s,t) = {}& \cos\beta(s,t)\,\cos\alpha_{\text{s}}(s,t)\,\cos\Delta\psi(s,t)\\ &+ \sin\beta(s,t)\,\sin\alpha_{\text{s}}(s,t)\end{aligned} \tag{21}$$

where β is the tilt of the solar panels, α_{s} is the solar altitude angle (i.e. the angle between the Sun's rays and the horizontal plane), and $\Delta\psi$ is the azimuth difference between the Sun's rays and the panels' orientation, defined as

$$\Delta\psi(s,t) = \psi_{\text{p}}(s,t) - \psi_{\text{s}}(s,t) \tag{22}$$

where ψ_{p} is the azimuth angle of the solar panels and ψ_{s} is the solar azimuth angle. If the panels are perfectly facing the Sun (i.e. the Sun lies on the vertical plane of the panels' normal), then $\Delta\psi(s,t) = 0$. The solar altitude angle α_{s} is the complement to the solar zenith angle θ_z, which is obtained from forecast data

$$\alpha_{\text{s}}(s,t) = \frac{\pi}{2} - \theta_{\text{z}}(s,t). \tag{23}$$

The second contribution to solar irradiance is from the Sun's rays being scattered by the atmosphere and is computed as

$$I_{\text{dif}}(s,t) = F_{\text{sky}}(s,t)\cdot\ I_{\text{d}}(s,t) \tag{24}$$

where F_{sky} is the fraction of the sky dome seen by the panels and I_{d} is the diffuse horizontal irradiance, i.e. the radiation at the Earth's surface from sunlight scattered by the atmosphere. The function F_{sky} depends on the tilt β and is computed as

$$F_{\text{sky}}(s,t) = \frac{1+\cos\beta(s,t)}{2}. \tag{25}$$

Finally, the last contribution to solar irradiance is from the reflection of sunlight on the ground, which is computed as

$$I_{\text{alb}}(s,t) = \rho(s,t)\,I_{\text{g}}(s,t)\,\big(1 - F_{\text{sky}}(s,t)\big) \tag{26}$$

where ρ is the ground albedo, i.e. the fraction of sunlight diffusely reflected by the ground, and I_{g} is the global horizontal irradiance (GHI), i.e. the total irradiance from the Sun on the ground.

4.2. Charging during the TTS

It is assumed here that there is only one TTS per day (e.g., a resting stop during the night). Then, (18) can be integrated over the duration of a stop to compute the energy obtained during that stop on a certain day d

$$E_{\text{sun}}(s) = \int_{t^s_{d,0}}^{t^s_{d,\text{f}}} P_{\text{sun}}(s,t)\text{d}t,\ \ s \notin \mathbb{S}_{\text{drv}} \tag{27}$$

where $[t^s_{d,0}, t^s_{d,\text{f}}]$ is the time interval of the stop in location s.

Since the problem is modeled in space domain, the energy comes all at once in one space sample when charging while the vehicle is standing still. This behavior can be modeled as an impulse between two time instants t_1 and t_2

$$\delta_{[t_1,t_2]}(t) = \begin{cases} 1, & \text{if } t_1 \le t \le t_2 \\ 0, & \text{otherwise.} \end{cases} \tag{28}$$

This looks like a Dirac impulse only in space domain (and if the vehicle does not move in $[t_1, t_2]$). In time domain, this looks like a rectangular impulse. However, such a function clearly introduces differentiability problems. Therefore, the impulse in (28) is approximated as the difference between two sigmoid functions as

$$\begin{aligned}\tilde{\delta}(t,t_1,t_2) = {}& \frac{1}{1+\exp\big(-\sigma(t-t_1)\big)} + \\ &- \frac{1}{1+\exp\big(-\sigma(t-t_2)\big)}\end{aligned} \tag{29}$$

where σ is the steepness of the sigmoids. This parameter introduces a trade-off: increasing it improves the approximation to (28) but raises the risk of non-differentiability. In a nutshell, the function "stretches" the impulse, spreading it over several samples. Having this, we can define the power obtained during an TTS as

$$P_{\text{tts}}(s,t) = \sum_{d=1}^{N_d} \frac{E_{\text{sun}}(s)}{t_{\tilde{\delta}}} \cdot \tilde{\delta}\big(t,\ \tau(s_d),\ \tau(s_d) + t_{\tilde{\delta}}\big) \tag{30}$$

where $t_{\tilde{\delta}}$ is the time duration of the smoothed impulse, and s_d is the location of the TTS reached during day d.

Let us unpack (30). The sum over all the days of the race is needed because, since time is a decision variable, we do not know in advance which day the stop refers to. The correct day will be selected by the function $\tilde{\delta}$, defined in (29). The elapsed time t, passed as an argument to $\tilde{\delta}$, will only be within one of the intervals $[\tau(s_d),\ \tau(s_d) + t_{\tilde{\delta}}]$, for $d = 1, \dots, N_d$, meaning that $\tilde{\delta}$ will be equal to 0 for all days of the race except for the one the stop refers to. The smoothed impulse is dimensionless, meaning that the quantity computed in (30) is dimensionally a power.

4.3. Charging while driving and during the LTS

The power obtained while driving can be computed as

$$P_{\text{drv}}(s,t) = \sum_{d=1}^{N_d} P_{\text{sun}}(s,\ t)\cdot\tilde{\delta}\big(t,\ \tau(s_{d,0}),\ \tau(s_{d,\text{f}})\big) \tag{31}$$

where $s_{d,0}$ and $s_{d,\text{f}}$ are, respectively, the first and last location reached during day d. This is the sum of the solar power obtained while driving for all days of the race. However, since P_{drv} is a function of s and t, it refers to a specific day, which is selected by the smoothed impulse function $\tilde{\delta}$, similarly to what is done in (30).

We now need to address the LTS, which is easier since, as opposed to the TTS, their location is known. The increase in SoC during an LTS in location s is given by

$$\delta\text{SoC}_{\text{lts}}(s) = \frac{E_{\text{sun}}(s)}{C_{\text{b}}V_{\text{oc}}(\text{SoC})},\ \ s \in \mathbb{S}_{\text{stop}} \tag{32}$$

meaning that the following applies for a generic LTS

$$\mathbf{x}(s^+) = \mathbf{x}(s) + \begin{bmatrix}0 & 0 & \delta\text{SoC}_{\text{lts}}(s)\end{bmatrix}^{\intercal},\ \ s \in \mathbb{S}_{\text{stop}} \tag{33}$$

where s^+ is the location right after the LTS.

The problem in (7) is then reformulated in space domain as

$$\min_{\mathbf{x},\mathbf{u},\boldsymbol{\epsilon}}\ \boldsymbol{J}(s) \tag{34a}$$

$$\text{s.t.: } \mathbf{x}(0) = \mathbf{x}_0, (6), (8) \tag{34b}$$

$$(15),\ \ s \notin \mathbb{S}_{\text{stop}} \tag{34c}$$

$$\mathbf{x}(s^+) = \mathbf{x}(s) + \delta\mathbf{x}_{\text{L}}(s),\ \ s \in \mathbb{S}_{\text{stop}} \tag{34d}$$

$$\mathbf{x}_{\min} \le \mathbf{x}(s) + \boldsymbol{\epsilon}_{\boldsymbol{x}}(s) \le \mathbf{x}_{\max},\ \ s \in [0, s_{\text{f}}] \tag{34e}$$

$$\mathbf{u}_{\min} \le \mathbf{u}(s) \le \mathbf{u}_{\max},\ \ s \in [0, s_{\text{f}}]. \tag{34f}$$

5. Results from case study: Solar-powered EV racing

The method introduced in this article is applied to a solar EV racing in the BWSC. One constraint from the official rules of the competition

Fig. 3. Path and LTS for the BWSC.

is that the vehicle may only drive from 08:00 to 17:00, i.e. the above-mentioned TTS. Another constraint is related to set checkpoints that need to be reached within a specified time and where the vehicle stops for 30 min, i.e. the above-mentioned LTS. The vehicle can charge with solar power during all stops, as long as there is sunlight. The set of locations for the LTS is known in advance and denoted by $\mathbb{S}_{\text{stop}}$, while the set of locations for the TTS is computed as a decision variable and denoted by $\mathbb{S}_{\text{T}}$. The path of the competition, together with all the LTS (blue circles), can be seen in Fig. 3.

During the stops, the solar panels were tilted towards the sun to maximize energy absorption. That is, $\Delta\psi$ (22) was minimized. This possibility is taken into account in the simulation by using a look-up table which maps day and hour of the day to solar irradiance, assuming the solar panels are oriented optimally.

5.1. Simulation results

All tests were run on a machine with 32 GB RAM, 1.8 GHz processor and 64-bit Windows 10. The problem in (7) was solved with IPOPT (Dikin, 1967), a solver based on the interior point method (Potra & Wright, 2000). CasADi (Andersson et al., 2018) was used as an interface to formulate the problem. Table 1 shows the parameters used during simulation. The route data, including slope θ and speed limits $v_{\max}$, was acquired through Google Maps and consists of around 3×10^4 points containing longitude, latitude and altitude.

All atmospheric inputs are sourced from a dataset supplied to all teams participating in the BWSC. The data consists of both live and forecast data, with a 5-min temporal resolution. The route is represented through about 30 000 points. In addition to this, a number of measurement points with solar panels is available to compute solar power according to Section 4.

The test run shown in the figures below is completed in about 47 h and 34 min, with an average speed of 63.07 km/h, 5 TTS and 9 LTS. Fig. 4 shows the speed profile for the test run. The samples are 3km long and the speed should be interpreted as the average speed over the sampling intervals, which is why it is strictly positive.

The sigmoid steepness σ in (29) should be chosen as high as possible while still guaranteeing numerical differentiability. Multiple tests were performed and the feasible range for σ was identified as $[4 \cdot 10^{-4}, 3.6 \cdot 10^{-3}]$, as the solver failed to converge to a feasible solution for values outside of this interval. The achieved cost decreases consistently as σ increases. A value of $\sigma = 3 \cdot 10^{-3}$ was chosen, as it is close but not exactly equal to the upper feasibility bound, ensuring approximation accuracy while maintaining some margin for numerical robustness. Also, further increases in the value do not lead to significant changes in the cost function. The computation time needed to solve (34) is on average around 1min and it does not exhibit monotonic behavior as σ varies. Based on these observations, σ is tuned by first identifying the feasibility region, and then selecting a value close to the upper bound of said region to ensure robust convergence and optimality.

Fig. 5 shows the SoC profile for the same test run, both in space (upper) and in time domain (lower). The lower bound on the SoC can be raised to increase robustness. Looking at the plot in space domain,

Table 1
Parameters used for simulation.

$m = 3 \times 10^2$ kg, $c_{\text{D}} = 1.98 \times 10^{-1}$, $\rho_{\text{air}} = 1.225$ kg m^{-3}
$A_{\text{f}} = 9.6 \times 10^{-1}$m^2, $g = 9.82$ m s^{-2}, $C_{\text{r}} = 5 \times 10^{-3}$
$A_{\text{p}} = 6$m^2, $\eta_{\text{p}} = 0.254$, $C_{\text{b}} = 1.08 \times 10^7$ J, $\mu_t = 1$
$\mu_\epsilon = 1$, $V_{\text{oc}} = 4 \times 10^2$ V, $R_{\text{dis}} = 3.04\ \Omega$, $R_{\text{chg}} = 7.36\ \Omega$
$\sigma = 3 \times 10^{-3}$, $\text{SoC}_{\min} = 0.15$, $\text{SoC}_{\max} = 0.95$
$s_{\text{f}} = 3 \times 10^6$ m, $a_{\max} = 0.8$ m s^{-2}, $a_{\min} = -0.8$ m s^{-2}
$\alpha_{\text{w}} = 7.5 \times 10^{-1}$, $N_d = 5$ days, $t_{\max} = 1.62 \times 10^5$ s
$t_{\text{ctrl}} = 1.8 \times 10^3$ s, $T_{\text{drv}}^{\text{day}} = 3.24 \times 10^4$ s, $T_{\text{drv}}^{\text{start}} = 2.88 \times 10^4$ s
$t_{\text{rise}} = 2.52 \times 10^4$ s, $t_{\text{set}} = 6.84 \times 10^4$ s, $t_\delta = 1.8 \times 10^3$ s
$\mathbf{T}_{\text{drv}}^{\text{tot}} = [0,\ 3.24,\ 6.48,\ 9.72,\ 12.96,\ 16.2]^\intercal \times 10^4$ s
$\mathbb{S}_{\text{ctrl}} = \{3.32,\ 5.88,\ 9.87,\ 12.1,\ 14.93,\ 17.66,\ 21.79,$
$24.32,\ 27.20\} \times 10^3$ m

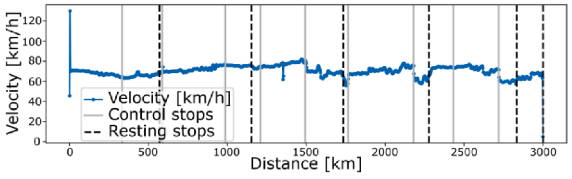

Fig. 4. Velocity profile from simulation.

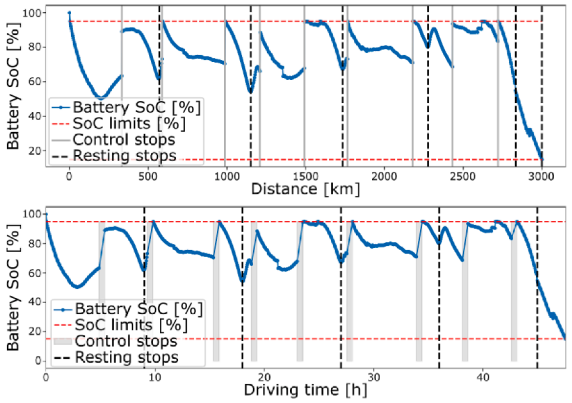

Fig. 5. SoC profile in space and in time domain from simulation.

we can see how the SoC "jumps" upward during the LTS, as the vehicle charges without moving (as per (33)). The actual charging process can be seen in the lower plot in time domain. It is interesting to note that the same thing does not happen for the TTS, even though the vehicle is charging while not moving also in that case. That is because the location of the TTS is not known in advance and instead of having just one space sample associated to these stops, we have an interval of them, which makes the charging process during these stops appear smoother. Fig. 6 shows the solar power profile for the same test run. The days of the race are clearly visible by the humps in the plot: the solar power starts low in the morning, reaches a maximum at midday, and then decreases again after that. It is interesting to notice the peaks that occur at every TTS (i.e. after 17:00 and before 08:00). Those are due to the fact that the vehicle can recharge for several hours without moving. As previously mentioned, the location of the TTS is not known in advance, meaning that we cannot associate an exact space sample to them. Instead, the behavior is approximated with the smoothed impulse function in (29), which is why the peaks are smoothed and why they occur over a few samples instead of only one.

5.2. Comparison between simulation results and telemetry data from the race

Fig. 7 shows the telemetry data measured during the race and compares it with the simulation results. The finish line was crossed after 45 h (about 5.69% lower than the simulation) and the average speed of

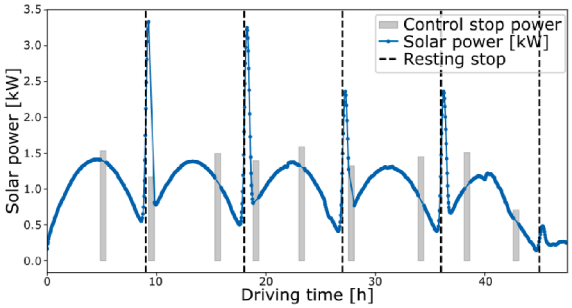

Fig. 6. Solar power profile as a function of driven time.

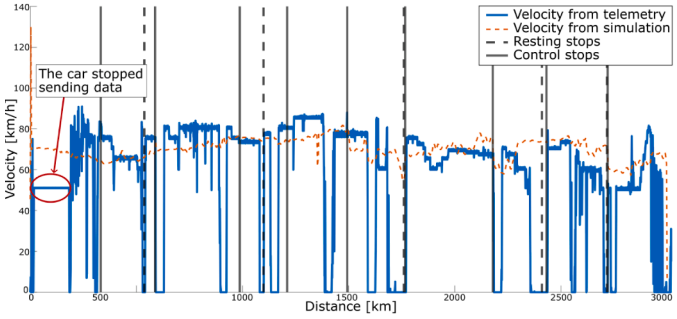

(a) Velocity profile.

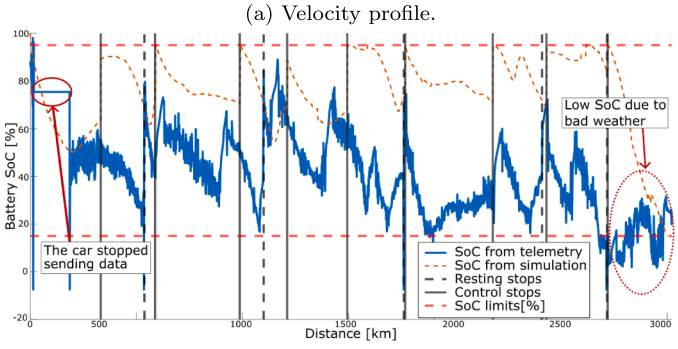

(b) SoC profile.

Fig. 7. Comparison between the telemetry data from the race and the results from simulation.

the vehicle during the race was around 67.33 km/h (about 6.75% higher than the simulation).

Fig. 7b highlights the mismatch between simulation results and race telemetry. A sensitivity analysis was conducted to assess the relative impact of the factors that contributed to this mismatch. The dominant source of discrepancy was found to be the open-loop nature of the simulation, whereas during the race the driving profile was recomputed on a daily basis, effectively resembling a shrinking-horizon model predictive control (MPC) strategy. This enabled the use of updated weather forecasts, which improved alignment with actual conditions. Indeed, when the simulation is executed retrospectively using the realized weather data from the race, the discrepancy between predicted and measured SoC is substantially reduced. The impact that accurate weather forecast has on the solution is particularly evident during the last day, when the weather was much more inclement than expected. This resulted in lack of sunlight, which is why the SoC is so low towards the end, as highlighted on the right side of Fig. 7b, and a higher mismatch with the forecast data.

The second most influential factor was the deterministic treatment of solar irradiance and speed limits in the model. The absence of stochasticity reduced robustness to forecast errors and variable traffic conditions, particularly in urban environments where speed fluctuations and stop-and-go traffic are more pronounced. Repeated acceleration phases in congested traffic increase energy consumption relative to steady-state driving due to inertial losses and drivetrain inefficiencies. Because the current model relies on deterministic, map-based speed limits and assumes free-flow conditions, it does not explicitly capture such traffic-induced speed oscillations, which may lead to underestimating the energy consumption in urban segments. However, the majority of the BWSC route consists of extra-urban roads, where speed profiles are closer to steady-state conditions and the present modeling assumptions are considered adequate. Moreover, since driving occurs during daytime hours and the vehicle can recharge while in traffic, continuous solar input partially compensates for temporary increases in traction power demand. As a result, the primary impact of traffic disturbances is expected to be on arrival time and local state evolution rather than on overall mission feasibility, which remains relatively robust under typical conditions. Nevertheless, arrival time and energy consumption predictions would be improved by introducing stochastic variations in admissible speed profiles to account for stop-and-go dynamics. In this case, the arrival time would become a stochastic variable, effectively transforming the problem into an optimal control problem with random stopping time (Boukas et al., 1990). In addition, incorporating stochasticity into the solar irradiance model (Eqs. (20), (24), and (26)) would enable a more realistic assessment of scenarios in which traffic congestion coincides with reduced solar input due to adverse weather. Another contributing factor was the limited availability of real-time communication between the team and the driver, which was restricted to specific time windows and prevented continuous feedback and online correction of the driving strategy.

Finally, measurement and numerical errors, as well as unforeseen technical issues encountered during the race, contributed to the mismatch to a lesser but comparable extent. Namely, the SoC obtained from telemetry data during the race is computed as

$$\mathrm{SoC}_{\mathrm{race}}(s) = \frac{f_{\mathrm{v2s}}(V_{\mathrm{oc}}^{\max}(s)) + f_{\mathrm{v2s}}(V_{\mathrm{oc}}^{\min}(s))}{2} \tag{35}$$

where $V_{\mathrm{oc}}^{\max}$ and $V_{\mathrm{oc}}^{\min}$ are, respectively, the maximum and minimum open circuit voltage measured at a location, and f_{v2s} is a function that maps the open circuit voltage to the corresponding value of state of charge ($f_{\mathrm{v2s}} : V_{\mathrm{oc}} \to \mathrm{SoC}$). The reason why the SoC occasionally drops below zero is that the measurements for the open circuit voltage are noisy, and the fact that the SoC is computed as the average between the maximum and the minimum values. Also, during the first day of the race, some problems occurred with the maximum power point trackers (MPPT, i.e. a system that maximizes energy extraction). This can be observed on the left side of both plots in Fig. 7, when the car stopped sending data. Namely, when the car starts from standstill and accelerates rapidly, the engine demands a lot of power, which causes the capacitors in the MPPTs to discharge and the MPPTs to shut down. To be able to address this problem during the race, an ON/OFF button for the MPPTs was installed in the vehicle, allowing the driver to manually turn them back ON, in case they shut down. What happened on the first day was that the MPPTs died at a red light and the driver tried to turn them back on during an uphill slope, which led to a power surge that caused the vehicle to be unable to send telemetry data until it was rebooted. This issue likely happened multiple times during the competition, which is why the speed measurements are sometimes equal to 0 over consecutive space instances, which should not be possible.

Overall, these findings indicate that implementing the optimization within a shrinking-horizon MPC framework would address the most significant sources of mismatch by enabling periodic re-optimization based on current telemetry, weather forecasts, and traffic conditions. In particular, we have identified the deterministic formulation of the current model as a major source of discrepancy between simulation and telemetry data, since the absence of stochasticity in the governing

equations limits its ability to account for uncertainties arising from inclement weather, forecast inaccuracies, imperfect real-time information, and traffic-dependent speed limits. To improve robustness, stochastic disturbances could be incorporated into the three components of solar irradiance (Eqs. (20), (24), and (26)), which are directly affected by forecast uncertainty, as well as into the speed limits to reflect traffic variability. Because solar irradiance directly determines P_{sun} and E_{sun}, introducing stochastic terms at this level would propagate uncertainty into the rest of the model, thereby reducing sensitivity to prediction errors and reducing the mismatch with telemetry data. Given that solving the optimization problem requires on average around 1 min for a sample size of 3 km, real-time implementation within an MPC framework is computationally feasible. However, its practical deployment would require reliable real-time communication between the driver and the team, which was not available during the race.

6. Conclusions and future work

In this work, the problem of optimizing trip time and energy management of a long-range solar-powered EV, subject to given spatio-temporal constraints, is formulated as an OCP through first principles modeling, and then solved through direct multiple shooting. The problem was modeled in space domain to remove location s from the states. This is advantageous for the LTS, as their location is known. Since that is not the case for the TTS, a smoothed impulse function was used to embed those constraints in the model without using integer variables and while still preserving differentiability. The output of the optimization is a driving profile which guarantees constraint compliance and race completion, while also minimizing driving time.

As a case study, the method was used to optimize the driving profile of a solar-powered vehicle competing in the BWSC, a 3 022 km race across the Australian outback. The spatio-temporal constraints dealt with in the method arise from the rules of the competition. The driving profile computed by the method was followed by the Chalmers Solar Team (as much as communication allowed) and it helped the team finish, something that only slightly more than half of the teams managed.

A sensitivity analysis was performed to identify which factors affect the most the mismatch between the simulation results and the race telemetry data. It was concluded that these factors could be addressed by incorporating the proposed method in a shrinking-horizon MPC scheme, which is computationally feasible given that the computational time needed to solve the problem is small relative to the length of the driving segments. Another further improvement is the introduction of stochasticity in the weather forecast and in the speed limits, to increase the method's robustness against uncertainty in the weather data and in the traffic conditions.

Additional future work is to further validate the method on other case studies, e.g., mission planning for solar-powered freight transport, where aspects like the driver having to take a break after many hours of driving (TTS) or the truck stopping to recharge at a station (LTS) need to be considered.

The method will be used by the Chalmers Solar Team to compare different designs for the vehicle to be used in the next iteration of the BWSC. This can be especially useful since solving the problem in (7) gives a concrete measure (i.e. the time it takes to complete the race) to objectively evaluate how the solar panel's inclination and shadowing affect the performance in relation to the aerodynamic losses. On the topic of shadowing, it would be useful to take into account the effect of trees close to the road which reduce solar irradiance.

CRediT authorship contribution statement

Lorenzo Montalto: Writing – review & editing, Writing – original draft, Supervision; **Nikolce Murgovski:** Writing – review & editing, Supervision, Software, Methodology, Formal analysis; **Timothy Jarebrant:** Writing – review & editing, Validation, Software.

Declaration of competing interests

The authors declare that they have no known competing financial interests or personal relationships that could have appeared to influence the work reported in this paper.

References

Andersson, J. A. E., Gillis, J., & Horn, G., et al. (2018). CasADi: A software framework for nonlinear optimization and optimal control. *Mathematical Programming Computation*, *11*(1), 1–36.

Billinton, R., & Bagen (2006). Reliability considerations in the utilization of wind energy, solar energy and energy storage in electric power systems. In *2006 international conference on probabilistic methods applied to power systems* (pp. 1–6).

Boukas, E.-K., Haurie, A., & Michel, P. (1990). An optimal control problem with a random stopping time. *Journal of Optimization Theory and Applications*, *64*(3), 471–480.

Deshpande, S. R., Gupta, S., Gupta, A., & Canova, M. (2022). Real-time ecodriving control in electrified connected and autonomous vehicles using approximate dynamic programing. *Journal of Dynamic Systems, Measurement, and Control*, *144*(1), 011111.

Dikin, I. I. (1967). Iterative solution of problems of linear and quadratic programming. *Soviet Mathematics Doklady*, *8*, 674–675.

Hamednia, A., Murgovski, N., Fredriksson, J., Forsman, J., Pourabdollah, M., & Larsson, V. (2023). Optimal thermal management, charging, and eco-driving of battery electric vehicles. *IEEE Transactions on Vehicular Technology*, *72*(6), 7265–7278.

Huang, Y., Ng, E. C. Y., Zhou, J. L., Surawski, N. C., Chan, E. F. C., & Hong, G. (2018). Eco-driving technology for sustainable road transport: A review. *Renewable and Sustainable Energy Reviews*, *93*, 596–609.

Kiehl, M. (1994). Parallel multiple shooting for the solution of initial value problems. *Parallel Computing*, *20*(3), 275–295.

Kirk, A. P. (2014). Solar photovoltaic cells: Photons to electricity. Academic Press.

Kish, R. (2023). Are electric vehicles really green? *Economic Affairs*, *43*(2), 275–286.

Li, G., Görges, D., & Wang, M. (2022). Online optimization of gear shift and velocity for eco-driving using adaptive dynamic programming. *IEEE Transactions on Intelligent Vehicles*, *7*(1), 123–132.

Li, J., Wu, X., Xu, M., & Liu, Y. (2024). Multiobjective eco-driving strategy for connected and automated electric vehicles considering complex urban traffic influence factors. *IEEE Transactions on Transportation Electrification*, *10*(4), 10043–10058.

Pevec, D., Babic, J., Carvalho, A., Ghiassi-Farrokhfal, Y., Ketter, W., & Podobnik, V. (2019). Electric vehicle range anxiety: An obstacle for the personal transportation (r)evolution? In *2019 4th international conference on smart and sustainable technologies (splitech)* (pp. 1–8).

Potra, F. A., & Wright, S. J. (2000). Interior-point methods. *Journal of Computational and Applied Mathematics*, *124*(1), 281–302. Numerical Analysis 2000. Vol. IV: Optimization and Nonlinear Equations.

Ritchie, H., Rosado, P., & Roser, M. (2020). Breakdown of carbon dioxide, methane and nitrous oxide emissions by sector. *Our World in Data*, . https://archive.ourworldindata.org/20260402-164039/emissions-by-sector.html

Sobczuk, S., & Borucka, A. (2024). Recent advances for the development of sustainable transport and their importance in case of global crises: A literature review. *Applied Sciences*, *14*(22), 10653 .

Zhang, Y., Wijeratne, L. O. H., Talebi, S., & Lary, D. J. (2021). Machine learning for light sensor calibration. *Sensors*, *21*(18), 6259.